THE JOURNAL OF PHYSICAL CHEMISTRY B

ARTICLE

pubs.acs.org/JPCB

Analysis of 5-Hydroxyisoflavones by Surface-Enhanced Raman Spectroscopy: Genistein and Methoxy Derivatives

Ryo Sekine,[†] Jitraporn Vongsvivut,[‡] Evan G. Robertson,[§] Leone Spiccia,[†] and Don McNaughton*[,†]

[†]School of Chemistry, Monash University, Wellington Road, Clayton, Victoria 3800, Australia

[‡]School of Life and Environmental Sciences, Deakin University, Pigdons Road, Waurn Ponds, Victoria 3217, Australia

[§]Department of Chemistry, La Trobe Institute for Molecular Science, La Trobe University, Bundoora, Victoria 3086, Australia

Supporting Information

ABSTRACT: A series of 5-hydroxy-isoflavones—genistein, biochanin A, prunetin, and 4′,7-dimethoxygenistein—have been studied by surface-enhanced Raman spectroscopy (SERS). Citrate reduced silver colloids were employed as a standard technique to measure SER spectra over a range of pH and concentrations. Density functional theory calculations were used to assist in determining the mode of interaction of isoflavones with the silver nanoparticles. It is revealed that biochanin A and prunetin interact with the silver nanoparticles upon deprotonation of the 7- and the 4′-OH groups, respectively, to show SERS activity. Correlations of their spectra with SERS of genistein strongly support the presence of multiple interaction modes involving both of the OH groups in genistein, in a similar manner to daidzein. Surprisingly, however, under these conditions, the 5-OH group was found to be noninteractive as revealed by attempts to measure SERS of 4′,7-dimethoxygenistein. This was attributed partly to the low solubility and, more importantly, to the influence of steric hindrance, caused by the position of the pendant phenyl ring, which prevented interaction with the Ag colloid surface. These results complement recent work on daidzein and formononetin and provide further insight into understanding the SER spectra of isoflavones.

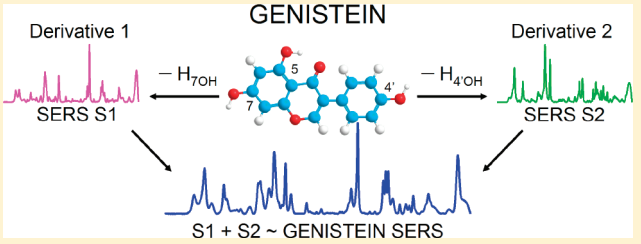

INTRODUCTION

Since the discovery of the enhancement of the Raman signal from pyridine adsorbed on a roughened electrode,[1] surface-enhanced Raman (SER) spectroscopy, or SERS, has become a prolific field of study with enormous advantages offered over conventional normal Raman (NR) spectroscopy. A combination enhancements arising from an electromagnetic mechanism (EM) due to localized surface plasmon resonance, and chemical mechanisms (CM) resulting from the molecule−metal interactions are accepted as the two major contributors to the Raman signal enhancements.[2−4] While SERS may be regarded as universal for species in the proximity of the metal under the EM,[5] the enhancements are greatest for the species closest to the metal surface. This is because the strength of electric field due to surface plasmon resonance is proportional to r^{-3} (r = distance) from the surface,[6] which creates a strong distance dependence on the EM enhancement (r^{-10}).[7] Moreover, CM, or specifically, the charge transfer (CT)[8] and the ground state nonresonant (CHEM)[9] enhancements require the molecule-metal interactions as a prerequisite. Thus, species with a stronger affinity toward the metal surface and preferentially adsorb will be subject to greater enhancement. As a consequence, the study of SERS on a new target begins with the search for a set of conditions that optimizes analyte adsorption, which tend to be molecule specific depending on the nature of the interaction.

We have recently reported a detailed SERS analysis on daidzein (4′,7-dihydroxyisoflavone) and formononetin (4′-methoxy-7-hydroxyisoflavone), which are two isoflavones that belong to a broader class of chemicals known as phytoestrogens.[10] The properties and interactions of this class of chemicals are of interest given the increasing awareness of their role in human health and their growing use as neutraceuticals. A number of potential health benefits have been identified including the prevention or reduced risk of cancer, heart disease, osteoporosis, and postmenopausal symptoms,[11−15] while conflicting reports exist on its role in increased thyroid disorders[16] and impaired male fertility.[17,18] Here, we examine four related isoflavones: genistein (4′,5,7-trihydroxyisoflavone), biochanin A (5,7-dihydroxy-4′-methoxyisoflavone), prunetin (4′,5-dihydroxy-7-methoxyisoflavone), and 4′,7-dimethoxygenistein (5-hydroxy-4′,7-dimethoxyisoflavone), which all possess a hydroxyl group at the C_5 position (Figure 1). A group of structurally related molecules, flavones, which have the phenol ring attached to the C_2 position of the chromone system, have also been the subject of previous SERS studies by several groups.[19−21] SERS of genistein and its derivatives, on the other hand, have not been published

Received: August 12, 2011
Revised: October 15, 2011
Published: October 19, 2011

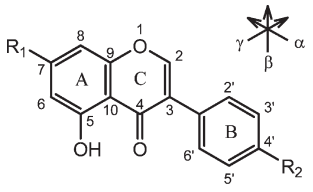

	R_1	R_2
a) Gstn	OH	OH
b) BchA	OH	OCH_3
c) Prtn	OCH_3	OH
d) Dmg	OCH_3	OCH_3

Figure 1. Molecular structure of the four 5-hydroxyisoflavones studied: (a) genistein (GSTN), (b) biochanin A (BCHA), (c) prunetin (PRTN), and (d) 4′,7-dimethoxygenistein (DMG). The labels α, β, and γ refer to the directions used for defining the vibrational ring modes.

anywhere to the best of our knowledge, apart from a paper by Bhandari et al.,[22] who used a selection of flavonoids, including daidzein and genistein, to test the efficacy of a new SERS active extraction filter to preconcentrate analytes and acquire their spectra.

Owing to its growing importance, various spectroscopic methods such as UV−visible,[23] infrared (IR),[23,24] and NR spectroscopy[25] have been used to study, in particular, genistein, due to its higher occurrence in the human diet as a major isoflavone found in soy beans. It is the aim of this study to extend the previous SERS study of isoflavones, and to lay the framework for possible future application to phytoestrogen analysis. In our previous study, it was revealed that the OH substitution pattern on the isoflavone backbone has a great influence on its interaction with the metal surface, and as a consequence, manifests a significant variation in the spectral profile.[10] The nature of this interaction was successfully probed by substituting one of the OH groups with a methoxy group, which in effect, eliminated one site of interaction, combined with density functional theory (DFT) calculations.

Computational methods have been used extensively to assist in the understanding of SERS. Within the static, time-independent methods, NR spectral simulations facilitate assignments on the experimental NR spectra that are useful in interpreting the SER spectra.[26−28] It has also been demonstrated that the simple addition of metal adatom (M/M^{n+}) is able to provide further insight into SERS. For example, energetically favorable metal−analyte complexes can be identified[29−31] and used to simulate the Raman spectra[32−36] and may be extended to incorporate metal clusters.[37−39] The latter techniques are able to provide some theoretical insight into wavenumber shifts on analyte−metal interaction[32−34,36,38] and, within limits, intensities,[37−39] which is an invaluable tool in SERS analysis. Furthering the approach to time-dependent (TD) theories such as TD-DFT can take these calculations beyond the static limit, enabling the additional inclusion of enhancements arising from EM (with larger clusters such as Ag_{20}), CT, and molecular resonance enhancements.[40−43]

In this paper, we adopt the use of static Raman calculations of the molecules complexed with adatoms (Ag^0 and Ag^+) to analyze the SERS of genistein and its derivatives. Due to the number of molecules examined in this study, the SERS analysis of the isoflavones only is treated in this paper, whereas the NR and IR analyses that form the necessary background to the work have been published separately.[44] The combined approach of experimental and computational investigations demonstrates another multimodal interaction mechanism for genistein, supported by comparison with its methoxy derivatives.

EXPERIMENTAL SECTION

Materials and Reagents. Genistein (GSTN, ≥99%) was purchased from LC Laboratories (MA, U.S.A.), Biochanin A (BCHA, 97.4%) and Prunetin (PRTN, ≥98.0%) are from Sigma-Aldrich (New South Wales, Australia), and 4′,7-dimethoxygenistein (DMG, 98%) is from ChemCollect GmbH (Remscheid, Germany). Stock solutions of 2.0 mM concentration were prepared in absolute ethanol (≥99.7% purity, Merck, Victoria, Australia) and working standards (10−100 μM) were prepared by further dilution of the stock solution. In the case of DMG, a 100 μM solution was directly prepared due to its poor solubility.

All glassware were cleaned by treatment with a 10% Pierce PCC-54 detergent solution (Thermo Fisher Scientific Inc., IL, U.S.A.), an alternative reported to be as effective as aqua regia in cleaning the glassware for SERS purposes.[19,45] They were subsequently sonicated for 5 min each in acetone and methanol and finally rinsed with 18.2 MΩ ultrapure water.

Silver (Ag) colloids used in the SERS measurements were prepared by reduction of silver nitrate (≥99.9999% $AgNO_3$, Sigma-Aldrich, New South Wales, Australia) with citrate as reported by Lee and Meisel.[46] The absorption spectrum was acquired periodically to monitor the colloid aggregation during synthesis. The colloid thus prepared had a turbid gray appearance with a λ_{max} = 414 nm.

Raman Spectroscopy and SERS Acquisition. All Raman and SERS measurements were carried out on a Renishaw Raman Microspectrometer RM2000 (Renishaw, New Mills, UK) equipped with a 782 nm NIR excitation laser and a thermo-electrical cooled CCD detector, between 1800 and 200 cm^{-1}. The 782 nm laser excitation was used to avoid any potential sample degradation from shorter wavelength lasers. The laser power measured at the sample was usually less than 1 mW, with 1 × 10 s accumulation. The normal Raman (NR) spectra were obtained from the powder samples as purchased (polycrystalline solid) and also from the solid dried from the stock ethanolic solutions (dried solid).

SER spectra were obtained with citrate-reduced Ag colloids in a manner previously described.[10] Briefly, the spectra were acquired from a drop of premixed 2:1:2 Ag colloid solution/sample solution (10−100 μM)/0.2 M KNO_3 aqueous solution mixture, with the laser focused by a 20× or 50× objective on the aggregates identified in the droplet. This aggregate formation and targeting were found to be critical in obtaining optimal SERS signals, typically accumulating on the edge of the droplets. Other anions including SO_4^{2-} (as Na_2SO_4), Cl^- (as NaCl) and ClO_4^- (as $NaClO_4$) were additionally tested as aggregating agents in the study. NO_3^- was the first anion of choice for consistency with previous work[10,19,20] and was found to be effective for GSTN and PRTN. However, the spectral quality from BCHA was poor and was improved by using SO_4^{2-}, which interestingly was similar to the behavior of formononetin, the 4′-methoxy derivative of daidzein. For SERS in acidic conditions, the pH of the aggregating agent was initially varied by diluting a 0.2 M HNO_3 solution with 0.2 M KNO_3 to keep the NO_3^- concentration constant over the series. Alkaline solutions were prepared by appropriately diluting a 0.2 M KOH solution. Where SO_4^{2-} was used, H_2SO_4 or NaOH solution was appropriately diluted with 0.2 M Na_2SO_4 to

keep the SO_4^{2-} concentration constant over the series. It should be noted that the reported pH is that of the final mixture used for SERS measurements, which contains 20% ethanol (v/v) as solvent for the analytes. The pH was measured before and after the addition of the organic component and the increase (as expected) was typically less than 0.3 pH units, which is much smaller than the pK_a differences of the OH groups of interest and was deemed negligible.

Computational Chemistry. In order to aid assignment of the observed SERS bands, normal vibrational modes and Raman activities of the molecules were computed and then correlated with the corresponding predictions for the complexed species. The details of the conformational search and the NR spectrum calculations are described elsewhere.[44] In brief, all stable conformers identified using the AM1 semiempirical method in the *Hyperchem* software (Version 8.0.4, Hypercube Inc., Gainesville FL, U.S.A.) were further optimized with DFT at the B3LYP level with 6-31+G(d) basis set using the *Gaussian 03* software[47] (Gaussian, Inc., Wallingford CT, U.S.A.).

To evaluate spectral shifts induced by complexation to the silver surface, calculations were performed on systems containing silver (Ag^0) atoms and ions (Ag^+). A mixed basis set was used where a 6-31+G(d) basis set was used for carbon, hydrogen, and oxygen and the SDD basis set with Stuttgart pseudopotentials[48] for silver. The lowest energy conformer identified in the neutral molecule was used for the modeling of the complex. However, in practice, the small energy differences (ΔE < 3.0 kJ mol^{-1} predicted in vacuo) would likely be negligible in solution, except for 5-OH orientation (ΔE > 50 kJ mol^{-1}) due to the strong internal hydrogen bonding to the nearby carbonyl group.[44,49,50] Energy barriers to torsional rotations at the $Ag^{0/+}$ attachment site were calculated using the appropriate conformations by potential energy scans with a loose convergence criterion in the *Gaussian 03* software.

Normal mode vibrations and Raman activities were computed on the final optimized structures and were used to simulate the experimental spectra, where the final intensities are calculated for 782 nm excitation ($\bar{\nu}_0$ = 12787 cm^{-1}) using the formula[51]

$$I_i = \frac{f(\bar{\nu}_0 - \bar{\nu}_i)^4 S_i}{\bar{\nu}_i \left[1 - \exp\left(-\frac{hc\bar{\nu}_i}{kT}\right)\right]} \quad (1)$$

where S_i is the calculated Raman activity for the i-th mode at $\bar{\nu}_i$ cm^{-1}; h, c, and k are the fundamental constants, and f is a normalization factor. The temperature T was assumed to be 298 K. A uniform scaling factor (SF) of 0.979 was used to be consistent with earlier work on daidzein and formononetin. The resulting rms values are quoted with the appropriate tables for the molecules. Scaling factors are commonly applied to calculated vibrational frequencies to correct for, among several factors, anharmonicity of the potential energy surface.[52] Note that the simulated Raman spectra in the figures were generated by applying 8 cm^{-1} Lorentzian broadening to the wavenumber values. As a result, the labeled values on the figures may be slightly shifted from the calculated values in the tables.

RESULTS AND DISCUSSION

As has been highlighted in a large number of SERS studies, the adsorption of the analyte on to the rough metal surface is often the key to successful SERS observation.[53−55] In many cases, there is a delicate equilibrium with other electrolyte components coexisting in the SERS solution. The analyte must therefore have a higher affinity toward the metal surface than other electrolyte species. Unmodified citrate reduced silver colloids are covered with remnant citrate on the metal surface,[54] which helps to attract positively charged targets such as rhodamine 6G to facilitate their SERS activity. In daidzein and formononetin which are weakly acidic, we observed the pH dependent nature of their SERS activity, where it was concluded that they needed to be deprotonated in order to adsorb preferentially over remnant citrate on to the silver surface.[10] Accordingly, interaction was found to occur via the sites of deprotonation, the acidic hydroxyl (−OH) groups, 7-OH in formononetin and additionally at 4′−OH in

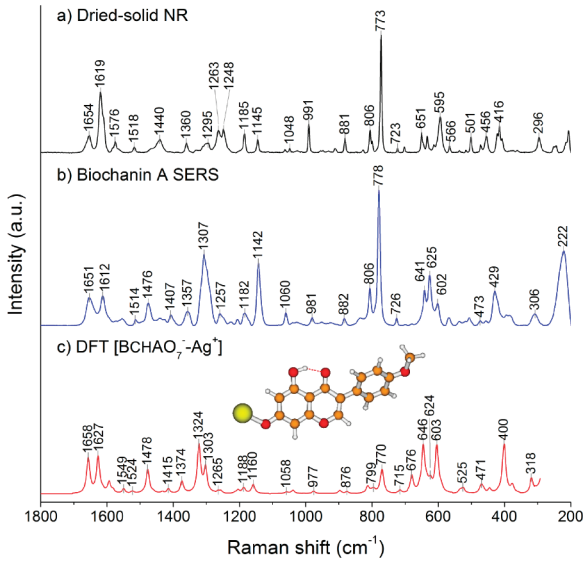

Figure 2. Experimental (a) dried solid-state Raman spectrum (from 2 mM solution), (b) SER spectrum of BCHA, and (c) simulated Raman spectrum of BCHA−Ag^+ complex, [$BCHAO_7^-$−Ag^+].

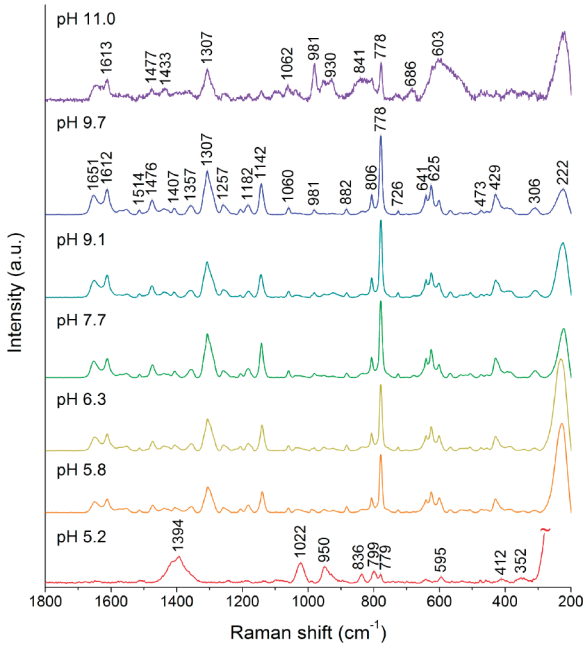

Figure 3. pH dependent SERS activity of BCHA. Citrate bands can be observed under acidic conditions while neutral to alkaline conditions give SERS of deprotonated BCHA.

Table 1. SERS Band Assignments for BCHA Using the Results of DFT Calculations on the Deprotonated BCHA−Ag^+ Complex, Mode Descriptions, and Their Corresponding Positions in the Neutral, Isolated BCHA Molecule

experimental (cm^{-1})[a]					DFT prediction (cm^{-1})[b]			
SERS		NR		Δ	[$BCHAO_7^-$−Ag^+]	BCHA	Δ	description of [$BCHAO_7^-$−Ag^+] mode [a,c]
306	w,br				318	352	−34	$\tau(C_4'OC_{Me}H_{IP}) + \tau(C_3C_1'C_6'C_5') + \nu(Ag{-}O_7)$ [g,h]
383	w,sh				375	376	−1	$\tau(C_9O_1C_2C_3) + \tau(C_{2'}C_{3'}C_{4'}O) + \tau(C_3C_{1'}C_{2'}C_{3'}) + \delta(C_3C_4{=}O)$ [g]
429[e]	m	406	w	23	400	402	−2	$\tau(C_9O_1C_2C_3) + \tau(OC_{4'}C_{5'}C_{6'}) + \tau(C_3C_{1'}C_{2'}C_{3'})$ [g]
		416	m	13	403	408	−5	$\tau(C_9O_1C_2C_3) + \delta(OC_5C_{10}) + \delta(C_7OAg) + \nu(Ag{-}O_7)$ [g,h]
455	vw	456	w	−1	446	448	−2	$\tau(C_9O_1C_2C_3) + \tau(C_5C_{10}C_4{=}O) + \tau(C_3C_{1'}C_{6'}C_{5'}) + \delta(C_{4'}OC_{Me})$ [g]
473	vw	472	w	1	463	465	−2	$\tau(HC_2C_3C_4) + \tau(C_5C_{10}C_4{=}O) + \nu(Ag{-}O_7)$ [g]
507	w	501	w	6	503	497	6	$\delta(C_8C_9C_{10}) + \delta(C_{4'}O_{4'}C_{Me}) + \delta(C_6C_5C_{10})$
536	vw	536	vw	6	536	534	2	$\gamma(CCC)^{16b}_{B\alpha}$
568	w	566	w	2	573	561	12	$\gamma(CCC)^{16b}_{B\alpha} + \delta(C_6C_7O) + \delta(C_4{=}O) + \delta(OC_5C_6) + \nu(Ag{-}O_7)$ [i]
602	m				603	610	−7	$\delta(C_6C_7C_8) + \delta(C_{2'}C_{3'}C_{4'}) + \delta(C_{4'}OC_{Me}) + \nu(Ag{-}O_7)$
625	s	613	w	12	624	613	11	$\nu(Ag{-}O_7) + \delta(C_6C_7C_8) + \delta(C_{3'}C_{4'}C_{5'}) + \nu(C_{1'}{-}C_3)$
641	m	634	w	7	646	629	17	$\tau(C_6C_7C_8H) + \tau(OC_5C_6H)$ [g]
726	w	723	vw	3	715	715	0	$\gamma(CCC)^{4}_{B}$
778[e]	vs	773	vs	5	769	768	1	$\gamma(C{-}H)^{11}_{B} + \tau(C_9C_{10}C_4{=}O) + \gamma(C_6{-}H)$ [g]
	vs				772	773	−1	$\gamma(C_6{-}H) + \tau(C_{1'}C_3C_4{=}O) + \tau(O_1C_9C_{10}C_4)$ [g]
806	m	798	w	8	799	806[f]	−7	$\gamma(C{-}H)^{10a}_{B\alpha} + \delta(C_{2'}C_{1'}C_{6'}) + \delta(C_9O_1C_2)$
882	w	881	w	1	876	871	5	$\delta(O_1C_2C_3) + \delta(C_4{=}O) + \nu(C_5{-}C_{10}) + \gamma(5\text{-}OH) + \delta(CCC)^{1}_{B}$
981	w	991	m	−10	977	984	−7	$\nu_{sym}(C_6{-}C_7, C_7{-}C_8) + \nu(C_7{-}O) + \nu_{sym}(C_9{-}O_1, O_1{-}C_2)$
1060	w	1062	w	−2	1058	1060	−2	$\nu(O_1{-}C_9) + \delta(C_2{-}H) + \nu(C{=}C)^{14}_{A}$
1142	s	1145	w	−3	1160	1152	8	$\delta(C_8{-}H) + \nu(C_7{-}O)$
1182[e]	w	1185	m	−3	1187	1186	1	$\delta(C{-}H)^{9a}_{B\alpha} + \delta(O_4'C_{Me}H_{OP})$
					1189	1188	1	$\delta(O_{4'}C_{Me}H_{OP}) + \delta(C{-}H)^{9a}_{B\alpha}$
1205	vw				1206	1196	10	$\delta(C_8{-}H) + \delta(C_6{-}H) + \nu_{asym}(O_1{-}C_2, C_4{-}C_{10})$
1257	w	1263	m	−6	1265	1267	−2	$\nu(C_4'\text{-}O)$
1293[d]	s	1295	w	−2	1303	1311	−8	$\delta(C_2{-}H) + \nu(C_{1'}{-}C_3) + \nu(C{=}C)^{14}_{A} + \nu(C_3{-}C_4) + \nu(C_7{-}O)$
1314[d]	s				1324	1325	−1	$\delta(C_8{-}H) + \delta(C_2{-}H) + \nu(C_5{-}O) + \nu_{asym}(C_4{-}C_{10}, C_5{-}C_{10}) + \nu(C_7{-}O)$
1357	w	1360	m	−3	1374	1367	7	$\nu_{asym}(C_6{-}C_7, C_7{-}O) + \nu(C_3{-}C_4) + \delta(C_2{-}H)$
1407	w				1415	1424	−9	$\nu_{sym}(C_7{-}O, C_5{-}O) + \nu_{asym}(C_3{-}C_4, C_4{-}C_{10}) + \delta(5O{-}H) + \nu(C{=}C)^{19bi,j}_{B\alpha}$
1476	m				1478	1503	−25	$\nu(C{=}C)^{19a}_{A\alpha} + \delta(5O{-}H) + \nu(C_7{-}O)$ [i,j,k]
1514	vw	1518	w	−4	1524	1524	0	$\nu(C{=}C)^{19a}_{B\alpha}$ [i,j]
1554	w				1549	1593	−44	$\nu(C{=}C)^{8b}_{A\beta}\ \nu(C_2{=}C_3) + \delta(5O{-}H)$
1612	m	1619	m,sh	−7	1627	1627	0	$\nu(C{=}C)^{8a}_{B\alpha}$ [i]
1651	m	1654	m	−3	1658	1664	−6	$\nu(C{=}C)^{8a}_{A\alpha} + \nu(C_2{=}C_3) + \delta(5O{-}H)$ [i]

[a] Labels used: vs, very strong; s, strong; m, medium; w, weak; vw, very weak; br, broad; and sh, shoulder. [b] All DFT predicted wavenumbers have been scaled uniformly by a factor of 0.9790. [c] Notations used: ν = stretch, δ = in plane bend, γ = out of plane bend, τ = torsion. Where a ring mode closely resembles those of benzene as shown by Alcolea Palafox,[67] Wilson numbering of the mode (1−20b) is shown in the superscript following a general description of the mode in parentheses, whereas the subscript indicates the corresponding ring (A, B, or C) and where applicable, direction (α, β, or γ as in Figure 1). Some modes are slightly different due to ring substituents and preference is then given to a more accurate description of the analyte complex. [d] 1307 cm^{-1} band was deconvoluted by Lorentzian curve fit to 1314, 1307, 1300, and 1293 cm^{-1} (data not shown). The two modes with significant $\nu(C_7{-}O)$ contribution are listed here. [e] Assigned to two merged modes. [f] The NR predicted position is highly sensitive to the selected conformers. [g] Torsional components (independent) experiencing the largest displacements according to the *Gaussian 03* program output are listed. [h] Output lists the internal hydrogen bonding "stretch" between 5-OH hydrogen and the carbonyl oxygen to be the largest contribution. [i] The motions appear as (CCC + CH). [j] Vibration degenerate according to Scherer. [k] Using Suter's description for phenolate anion,[57] ν_5 = 1476 cm^{-1}.

daidzein. Such behavior supports the description of anion adsorption on citrate reduced silver colloids as the competitive binding by Bell et al.[53]

Surface Enhanced Raman Spectroscopy of Biochanin A. BCHA has two OH groups at the C_5 and C_7 positions that can potentially deprotonate to give negatively charged species. Comparing the NR and SER spectra of BCHA (Figure 2), although many peaks appear to remain well aligned (e.g., 1619, 1518, 1185, 1145, 881, 773, and 566 cm^{-1} in the NR spectrum), a significant change in the spectrum indicative of a chemical interaction with the surface is clearly evident. As was previously established with formononetin,[10] the 7-OH (pK_a ~7.2)[56] is capable of interacting with the silver surface upon deprotonation and with a similar behavior observed in the pH dependence (Figure 3), the initial study was concerned with this site of interaction. Following a potential energy scan about the [ring A]−C_7−O^-−Ag^+ torsion, it was found to have an energy barrier comparatively higher (ca. 7.3 kJ mol^{-1}) than in the case of

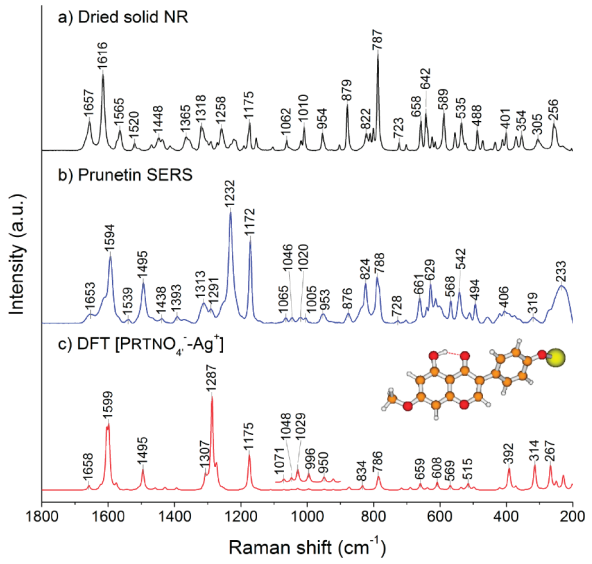

Figure 4. Experimental (a) dried solid-state Raman spectrum (from 2 mM solution), (b) SER spectrum of PRTN (pH 10.2), and (c) simulated Raman spectrum of the PRTN−Ag^+ complex, [$PRTNO_{4'}^-$−Ag^+].

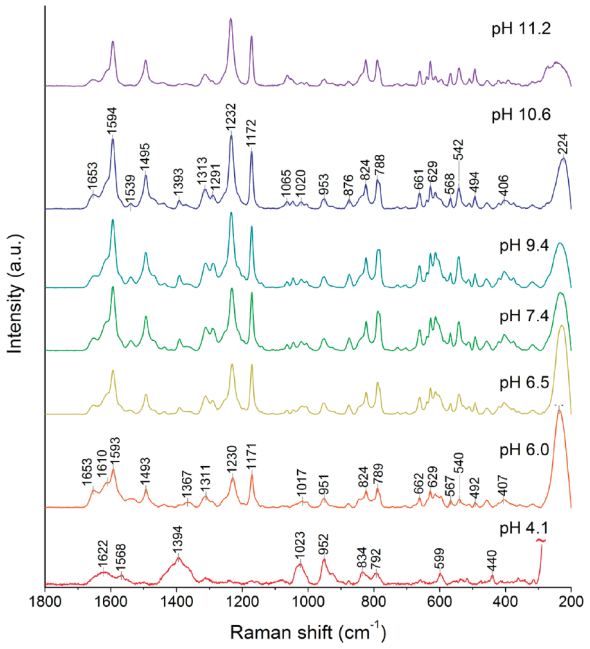

Figure 5. pH dependent SERS of PRTN. Variation in the relative intensities can be observed at low pH, which reappears in highly alkaline solutions.

formononetin (<4 kJ mol^{-1}) and was therefore expected to be more significant in its attachment orientation. Thus, the SER spectral assignment for BCHA is based on the lowest energy conformer, with Ag^+−O^- bond distance and Ag^+−O^-−[ring A] interior and dihedral angles of 2.08 Å, 121°, and 6° respectively: the Ag^+ slightly offset from the plane of ring A. The predicted Raman spectrum of the complex [$BCHAO_7^-$−Ag^+] is shown in Figure 2 and the SERS band assignment based on this structure is in Table 1. The rms deviation value according to the table is 10.7 cm^{-1}.

Vibrational analysis of the phenolate anion[57] and its Li^+ and Na^+ complexes[58] has shown that the ring stretching mode (19a) at 1483 cm^{-1}[59] (referred to as ν_5 in Suter et al.[60] and henceforth ν_5-type in this article) exhibits some C−O stretching character and is shifted from 1501 cm^{-1} in the neutral phenol.[61] We observed a similar shift in SERS of phenol, from 1501 cm^{-1} in the neutral solid-state NR to 1473 cm^{-1} in SERS, indicating its interaction as a phenolate (data not shown). Moreover, the mode with the strongest C−O stretching character in phenolate (ν_6) was found to be highly sensitive to the intermolecular interactions with Na^+ and Li^+.[58] We have found a similar behavior also with Ag^+, where in this case the length and torsion affected the DFT predicted C−O stretching wavenumber ($\Delta_{max} \approx 40$ cm^{-1}), whereas ν_5 remained consistent ($\Delta_{max} \approx 15$ cm^{-1}).

In the SER spectrum of BCHA, the ν_5-type band of ring A at 1476 cm^{-1} is a strong evidence for a C_7−O^-−Ag^+ interaction, supported by the observations on phenol, and with a similar shift of −32 cm^{-1} predicted by DFT (band not observed in experimental NR). On the other hand, the same band in ring B at 1514 cm^{-1} has only a modest shift from 1518 cm^{-1} in the NR since the methoxy group is not capable of interacting in the same manner. For the ν_6-type band, the 1307 cm^{-1} band in BCHA is expected to have a contribution from the C_7−O stretching mode, and the breadth may be partially accounted for by the sensitive nature of this mode to the interaction geometry. However, we could not isolate a single mode appropriate for such a simple description due to coupling to many other vibrations of the complex, and the band itself has several overlapping peaks: 1314, 1307, 1300, and 1293 cm^{-1}. Finally, an intense, broad band appears in the 210−240 cm^{-1} region for phenol and BCHA (and also for other derivatives). This was not studied in detail due to the presence of the colloid background but are most likely to arise from vibrations involving ν(Ag−O) of the probe molecules.[62]

An alternative site of interaction with the metal surface is at the 5-OH position, which was expected to chelate upon deprotonation. However, DFT predictions on species chelated to Ag^+ do not agree with the experimental SER spectrum (Supporting Information, Figure S1). For reasons that will also be discussed later, it appears that 5-OH does not contribute to analyte−metal interactions under these conditions.

Surface Enhanced Raman Spectroscopy of Prunetin. The complement of BCHA is prunetin (PRTN), where the 7-OH group is replaced with a methoxy group instead of the 4′-OH, thus blocking the C_7−O while permitting the $C_{4'}$−O to interact with the silver surface. The 5-OH remains unchanged and potentially available for further interactions.

As with BCHA, there is a dramatic change between the NR and SER spectra of PRTN, indicative of a structural change upon interaction with the surface (Figure 4). Although the pK_a of the 4′-OH group is ca. 8.3,[63] the SER spectrum of PRTN can be observed at pH 6.0 through to pH 11.2, with the major bands appearing in all spectra (Figure 5). It is well-known that the pK_a may be lowered in the presence of an interacting metal, and this may be the reason for the SERS observation at lower pH. Accordingly, the simple Ag^+ interaction DFT model on the PRTN anion deprotonated at 4′-OH was studied. Such optimized models of PRTN complex [$PRTNO_{4'}^-$−Ag^+] had an Ag^+−O^- bond distance of 2.07−2.08 Å and an Ag^+−O^-−$C_{4'}$ angle of 121−125°, depending on the dihedral angle about Ag^+−$O_{4'}^-$−[ring B]. The torsional energy barrier about this dihedral angle was less than 3 kJ mol^{-1}, which was considered to

dx.doi.org/10.1021/jp207730g |J. Phys. Chem. B 2011, 115, 13943–13954

Table 2. SERS Band Assignments for PRTN Using the Results of DFT Calculations on the Deprotonated PRTN−Ag^+ Complex, Mode Descriptions, and Their Corresponding Positions in the Neutral, Isolated PRTN Molecule

experimental (cm^{-1})[a]					DFT prediction (cm^{-1})[b]			
SERS		NR		Δ	[$PRTNO_4'^-$−Ag^+]	PRTN	Δ	description of [$PRTNO_{4'}^-$−Ag^+] mode [a,c]
319	m				314			$\nu(Ag{-}O_{4'}) + \tau(OC_{4'}C_{5'}C_{6'})$ [g]
406	m	371		35	392	372	20	$\tau(C_{5'}C_{6'}C_{1'}C_3) + \tau(C_9O_1C_2C_3) + \tau(C_{3'}C_{4'}OAg)$ [g]
457	w	472	w	−15	452	463	−11	$\tau(O_1C_2C_3C_4) + \tau(C_5C_{10}C_4{=}O)$ [g]
494	m				498			$\gamma(CCC)^{16b}_{B\alpha} + \tau(C_5C_{10}C_4{=}O) + \delta(C_{3'}C_{4'}O) + \delta(C_{4'}OAg)$
512	w	535	s	−23	515	528	−13	$\gamma(CCC)^{16b}_{B\alpha} + \delta(C_3C_4C_{10}) + \delta(C_9O_1C_2) + \nu(Ag{-}O_4')$ [j]
542	m	523	w,sh	19	536	523	13	$\gamma(CCC)^{16b}_{B\alpha} + \nu(Ag{-}O_{4'})$ [j]
568	w,br	555	m	13	569	552	17	$\delta(OC_5C_6) + \delta(C_2C_3C_4) + \gamma(CCC)^{16b}_{B\alpha} + \nu(Ag{-}O_{4'})$ [j]
614	m	615	w	−1	615	611	4	$\tau(HC_8C_9C_{10}) + \tau(HC_6C_5C_{10}) + \tau(C_9O_1C_2C_3)$ [g]
629	s	589	s	40	608	585	23	$\delta(OC_7C_8) + \delta(O_1C_2C_3) + \nu(C_9{-}C_{10}) + \nu(Ag{-}O_{4'})$ [j]
639	w	642	s	−3	637	638	−1	$\tau(HC_6C_7C_8) + \tau(OC_5C_6H) + \delta(CCC)^{6b\,g}_{B\alpha}$
661	m	658	m	3	659	654	5	$\delta(C_6C_7O) + \delta(C_{3'}C_{4'}C_{5'}) - \delta(OC_5C_{10}) + \nu(Ag{-}O_{4'})$ [j]
703	vw	702	w	1	690	684	6	$\gamma(CCC)^4_A + \tau(C_{1'}C_3C_4{=}O)$
728	vw	723	w	5	716	713	3	$\gamma(CCC)^4_B$
782[d]	m,sh				782	770	12	$\tau(O{=}C_4C_{10}C_5) + \tau(O_1C_2C_3C_4) + \gamma_{sym}(C_{5'}{-}H, C_{6'}{-}H)$
788	s	811	m	−22	787	801	−14	$\gamma(C{-}H)^{10a}_{B\alpha}$
824	s	822	m	2	834	820	14	$\delta(C_{2'}C_{1'}C_{6'}) + \nu(C_{4'}{-}O) + \nu_{sym}(C_{3'}{-}C_{4'}, C_{4'}{-}C_{5'})$
876	w	879	s	−3	874	870	4	$\delta(O_1C_2C_3) + \delta(C_4{=}O) + \gamma(5O{-}H) + \delta(CCC)^1_B$
953[e]	w,br				947	931	16	$\tau(HC_{5'}C_{6'}H)$
		954	m	−1	950	956	−6	$\nu_{sym}(C_6{-}C_7, C_7{-}C_8) + \nu_{sym}(C_7{-}O, O{-}C_{Me}) + \nu_{sym}(C_9{-}O_1, O_1{-}C_2)$
1005	vw	1010	m	−5	996	1006	−10	$\delta(C{-}H)^{18a}_{B\alpha}$
1020	vw	1019	w	1	1029	1024	5	$\nu(C_{Me}{-}O) + \nu_{sym}(C_{1'}{-}C_{2'}, C_{1'}{-}C_{6'}) + \nu_{sym}(O_1{-}C_2, C_3{-}C_4)$
1046	vw				1048	1051	−3	$\nu(O_1{-}C_9) + \delta(C_8C_9O_1) + \delta(C_6{-}H) + \delta(C_8{-}H)$
1065	vw	1062	w	3	1071	1062	9	$\nu(O_1{-}C_9) - \nu(C_3{-}C_4) + \nu(C_{Me}{-}O) + \delta(C_8{-}H)$
1172	vs	1178	w	−6	1175	1185	−10	$\delta(C{-}H)^{9a}_{B\alpha}$
1232	vs	1272	m,sh	−40	1287	1267	20	$\nu(C_{4'}{-}O)$ [k]
1255[d]	m,sh	1258	s	−3	1253	1257	−4	$\nu(C_{1'}{-}C_3) - \nu(O_1{-}C_2) - \nu(C_4{-}C_{10}) - \nu(C_7{-}O)$
1291	m	1291	m	0	1300	1303	−3	
1313	m	1318	s	−5	1307	1313	−6	$\delta(C_2{-}H) + \nu(C_3{-}C_{1'}) + \delta(C_{2'}{-}H) + \delta(C_{3'}{-}H)$
1372	vw	1365	m	7	1362	1364	−2	$\delta(C_2{-}H) + \nu(O_1{-}C_9)$
1393	w				1394	1391	3	$\nu(C{=}C)^{14}_A + \nu(5O{-}H) + \nu(O_1{-}C_9) - \nu(C_3{-}C_4)$
1438	vw	1436[f]	w	2	1429	1442	−13	$\nu(C{=}C)^{19b}_{B\alpha}$ [h,i]
1495	s	1520	w	−25	1495	1524	−29	$\nu(C{=}C)^{19a}_{B\alpha} + \nu(C_{4'}{-}O)$ [k]
1539	vw	1565	m	−26	1543	1597	−54	$\nu(C{=}C)^{8b}_{B\beta}$
1568[d]	w,sh				1575	1573	2	$\nu(C{=}C)^{8b}_{A\beta} + \nu(C_2{=}C_3) + \delta(5O{-}H)$
1594	vs	1616	vs	−22	1605	1629	−24	$\nu(C{=}C)^{8a}_{B\alpha}$ [h,k]
1615[d]	m,sh				1623	1620	3	$\nu(C_4{=}O) + \nu(C_2{=}C_3) + \nu(C{=}C)^{8a}_{A\gamma}$ [h]
1653	w	1657	s	−4	1658	1664	−6	$\nu(C{=}C)^{8a}_{A\alpha} + \nu(C_4{=}O) + \nu(C_2{=}C_3)$ [h]

[a] Labels and notations as per Table 1. [b] All DFT predicted wavenumbers have been scaled uniformly by a factor of 0.9790. [c] Some modes are slightly different to the equivalent NR description. In such cases, preference is given to a more accurate description of the analyte complex. [d] Shoulder peak revealed by Lorentzian curve fitting. [e] Assigned to two merged modes. [f] NR assignment is tentative. [g] See Table 1. [h] The motions appear as (CCC + CH). [i] Vibration degenerate according to Scherer. [j] NR equivalent modes are slightly different due to either $\nu(Ag{-}O4')$ contribution or $\tau(C_{Me}OC_6C_7)$ orientation ($\Delta E \approx 1$ kJ mol^{-1}). [k] Using Suter's description[57] for phenolate anion: ν_4 = 1594 cm^{-1}, ν_5 = 1495 cm^{-1}, and ν_6 = 1232 cm^{-1}.

be insignificant and thus the DFT prediction was selected based on rms of peak positions. In addition, some relative intensity changes were observed as the pH is varied from acidic to alkaline conditions that could not be easily accounted for. It is possible that there may be orientation changes on the surface, possibly related to the third deprotonation of the surface citrate (pK_{a3} 6.41).[64] In order to assign the observed bands, the average spectrum was used for the analysis.

The best overall match was obtained from a complex with bond length, angle, and torsion of 2.07 Å, 123°, and 65.3°, respectively, and its comparison is shown in Figure 4. The SERS band assignment based on this model is presented in Table 2. As can be seen, the phenolic ν_5-type mode of the B-ring is shifted from 1520 cm^{-1} in the NR to 1495 cm^{-1} in SERS (1524 → 1495 cm^{-1} in DFT), which supports the interaction of $C_{4'}$-O^- with the Ag surface. Other major bands are well reproduced with the DFT calculation, with 1594 (1605 in DFT, but part of overlapping bands), 1313 (1307), 1172 (1175), and 788 (787, overlap with 782) cm^{-1} in good agreement. The 1232 cm^{-1} band is, however, poorly predicted at 1287 cm^{-1}, which is

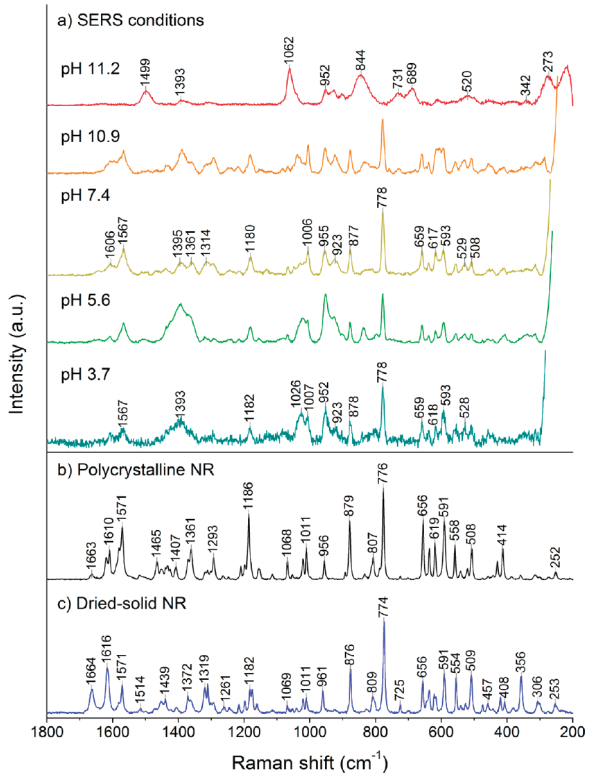

Figure 6. Spectra of DMG under (a) SERS conditions, (b) polycrystalline solid-state NR, and (c) dried solid-state NR (from 100 μM solution). Only a small variation is observed over the pH range in SERS, whereas the major bands are still observable at highly acidic pH.

assigned to the sensitive ν_6-type stretching of the $C_{4'}$—O. The final rms value for the assignments in Table 2 was 11.37 cm^{-1} (or 7.44 without the C—O stretch).

Again, deprotonation and the subsequent interaction with $Ag^{0/+}$ at the 5-OH position result in different predicted spectra which are not in agreement with the experimental spectrum, and thus not included in the analysis.

SERS Attempt on 4′,7-Dimethoxygenistein. In order to determine whether the 5-hydroxyisoflavones are also interacting with Ag surface via the 5-OH site, another derivative of GSTN with the 4′- and 7-OH groups both substituted with a methoxy group was studied. This compound, 4′,7-dimethoxygenistein (DMG), has only one possible site of interaction at the 5-OH. Due to the strong internal hydrogen bonding, it has a considerably high pK_a value of 11.0 (in 10% ethanol solution). Related compounds 5-hydroxyflavone and GSTN have pK_a values of 11.5[63] and 13.1, respectively where the latter has a higher value because this deprotonation process involves the formation of a trianionic species.

Previous studies on 5-hydroxyflavone[19] and alizarin,[65,66] molecules that share the same structural motif (OH with β-carbonyl group), have revealed that chelation to the Ag surface is likely to occur following 5-OH deprotonation. Alizarin in particular, shows a remarkable affinity to the Ag surface such that it can be observed in SERS at a much lower pH of 5.5 than its pK_a (11.5 in DMSO/water), providing evidence that the acidity of a proton can be dramatically changed in the presence of the Ag surface. Furthermore, DFT prediction of the Raman spectrum of 5-hydroxyflavone-Ag^+ chelation product agrees convincingly with the experimental SER spectrum with a predicted ν_{asym}(C═O, C—O^-), which is also coupled to an in-plane ring AC stretch, at 1433 cm^{-1} (1431 cm^{-1} by experiment[19]). Although Teslova et al. proposed a slightly different assignment based on the free, neutral molecule (as ring A, CC stretch),[19] the deprotonated model follows strongly from the accumulated evidence with our work on isoflavones.[10] It was thus expected that the 5-OH in DMG may also deprotonate and form a chelating product, DMG—Ag^+, with the surface even at a moderate pH, with the ν_{asym}(C═O, C—O^-) predicted at 1415 cm^{-1} (Supporting Information, Figure S3).

However, the experimental spectra of DMG under SERS conditions do not support the presence of a chelating product. As shown in Figure 6, in spectra over the pH range of 3.7 and 11.2, it is clear that the SER spectral profile of DMG is significantly different than any of the other isoflavones studied here. At very acidic pH (3.7), where all other isoflavones do not show SERS activity, the DMG marker band at 778 cm^{-1} is still observed. The change in the spectrum at pH 11.2 shows the loss of the analyte spectrum with only a band assignable to NO_3^- at 1062 cm^{-1} (confirmed by comparing with SO_4^{2-} aggregating agent at 982 cm^{-1}) and some colloid background. The latter behavior was seen in other isoflavones and has been attributed to the high concentration of hydroxides in the alkaline environment, forming oxides on the silver surface. The S/N levels of the spectra are ca. 2 orders of magnitude lower on average than at lower pH, and spectral interferences from the colloid are overwhelmingly present. Increasing the concentration above 20 μM only resulted in the precipitation of the analyte due to its poor solubility.

In fact, the NR (polycrystalline solid) and SER spectra of DMG are very similar with only minor band shifts, and the bands are sharp compared to the other isoflavone spectra. In consideration of this resemblance and the above factors, it is proposed that the spectra acquired are simply of DMG molecules that have physically adsorbed in the vicinity of the Ag nanoparticles due to its poor solubility in the solvent. The nanoparticles therefore remain coated with the citrate, and DMG molecules do not chemically interact with the metal surface. The combination of the inability to displace citrate from the surface and the lack of interaction would result in a low SERS enhancement. Based on this assumption, a tentative assignment of the SER spectrum is shown in Table 3, correlating directly to the NR spectrum and to the DFT predictions on the free molecule (rms = 7.1 cm^{-1}). A possible reason contributing to this result is steric hindrance caused by the B ring which prevents effective interaction between the hydroxyl group and the Ag surface. However, further investigation would be necessary to reach a definitive conclusion. It should also be noted here that the NR spectrum of the polycrystalline solid is slightly different to that of the dried solid (Figure 6), much like the behavior of GSTN.[44]

This result would imply that BCHA and PRTN are unlikely to interact at the 5-OH site. Spectral evidence in the experimental SERS is inconclusive, since the symmetric and antisymmetric ν(C_4═O, C_5—O^-), which are predicted at 1569 and 1417 cm^{-1} respectively for the chelating PRTN are both missing from the SER spectra (Supporting Information Figure S2). The γ(5-OH) mode, predicted to be present at 876 cm^{-1} if the compound does not deprotonate at the C_5 position is obscured by more intense in-plane ring C and B vibrational modes, predicted at 875 cm^{-1} and observed at 876 cm^{-1}. The δ(5-OH) mode is coupled to various in-plane ring vibrations and cannot be isolated in the

Table 3. Correlation of SERS and NR Bands of DMG and Their Descriptions

experimental (cm^{-1})[a]					DFT prediction	
SERS		NR[b]		Δ	position (cm^{-1})[c]	description[a,d]
508	w	508	m	0	501	$\delta(C_8C_9O_1) - \delta(C_7C_8H) + \delta(CCC)^{6a}_{B\alpha}$
529	w	520	w	9	525	$\gamma(CCC)^{16b}_{B\alpha}$ [f]
557	w	558	m	−1	553	$\gamma(CCC)^{16b}_{B\alpha} + \delta(C_6C_5C_{10}) - \delta(C_5C_6C_7)$ [f]
593	m	591	s	2	584	$\delta(C_6C_5C_{10}) + \delta(C_7OC_{7Me}) + \nu(C_9{-}C_{10}) + \nu(C_5{-}O) + \nu(O_1{-}C_9)$
617	m	619	m	−2	613	$\tau(HC_8C_9C_{10}) + \tau(HC_6C_5C_{10}) + \tau(C_9O_1C_2C_3)$ [e]
639	w	636	m	3	635	$\tau(HC_6C_7C_8) + \tau(OC_5C_6H) + \delta(CCC)^{6b}_{B\alpha}$ [e]
659	*m*	656	s	3	652	$\delta(OC_7C_8) + \delta(OC_5C_6) - \delta(O_1C_9C_8) + \tau(C_6C_7C_8H)$
778	s	776	vs	2	768	$\tau(C_{1'}C_2C_4O) + \tau(C_4C_{10}C_5O) + \delta(C_9O_1O_2) + \nu(C_4{-}C_{10})$
877	m	879	s	−2	869	$\delta(O_1C_2C_3) + \delta(C_4{=}O) + \nu(C_5{-}C_{10}) + \delta(CCC)^{1}_{B}$
923	w					*citrate band*
955	m	956	m	−1	956	$\nu_{sym}(C_6{-}C_7, C_7{-}C_8) + \nu_{sym}(C_7{-}O, O{-}C_{7Me}) + \nu_{sym}(C_9{-}O_1, O_1{-}C_2)$
1006	m	1011	m	−5	1003	$\delta(C{-}H)^{18a}_{B\alpha}$
1067	w	1068	m	−1	1064	$\nu(O_1{-}C_9) - \nu(C_3{-}C_4) + \nu(C_{7Me}{-}O) + \delta(C_8C_9C_{10})$
1180	m	1186	s	−6	1186	$\delta(C{-}H)^{9a}_{B\alpha}$
1294	w	1293	m	1	1307	$\nu_{asym}(C_{1'}{-}C_{6'}, C_{1'}{-}C_{2'}) + \delta(C{-}H)^{3}_{B} + \delta(5O{-}H)$
1314	w	1311	w	3	1321	$\nu(C{=}C)^{14}_{B}$
1361	w	1361	m	0	1365	$\delta(C_2{-}H) + \nu_{asym}(C_2{-}C_3, C_3{-}C_4)$
1395	w					citrate band
1567	m	1571	s	−4	1572	$\nu(C{=}C)^{8b}_{A\beta} + \nu(C_2{=}C_3) + \delta(5O{-}H)$
1606	w	1610	m	−4	1621	$\nu(C_2{=}C_3) + \nu(C_4{=}O) + \nu(C{=}C)^{8b}_{A\beta}$

[a] Labels and notations as per Table 1. [b] Peaks from the solid, crystalline phase. [c] All DFT predicted wavenumbers have been scaled uniformly by a factor of 0.9790. [d] Mode descriptions of the free, neutral molecule. [e] As per Table 1. [f] The motions appear as (CCC + CH).

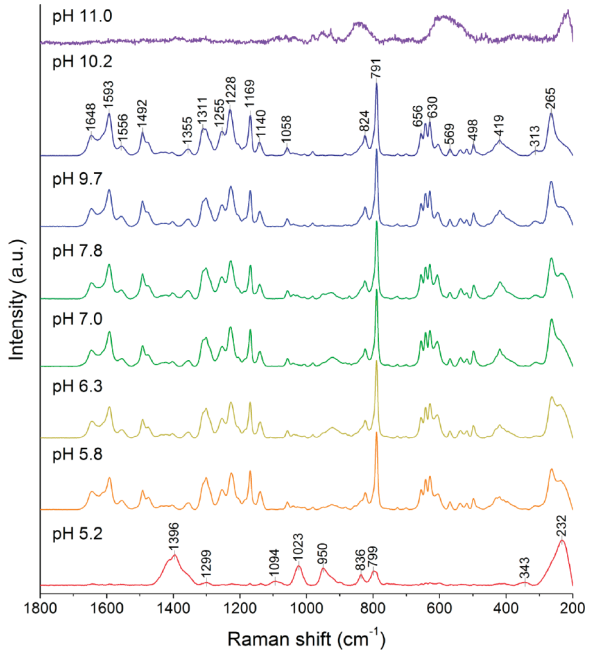

Figure 7. pH dependent SERS of GSTN. Similar behavior to the derivatives BCHA and PRTN is observed.

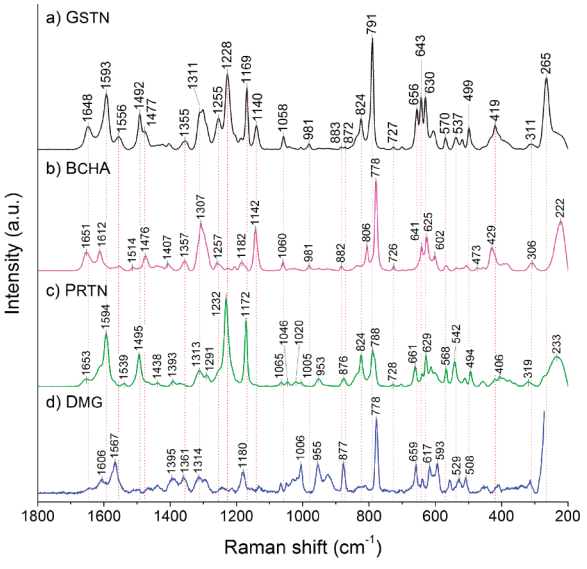

Figure 8. SERS comparison of (a) GSTN, (b) BCHA, (c) PRTN, and (d) DMG. An excellent correlation exists between the spectra of GSTN and their derivatives except for DMG where an alternative adsorption mechanism is proposed.

spectra. A similar argument can be drawn for BCHA. It is thus proposed that the primary interaction is at the deprotonated OH groups at the C_7 and C_4' positions of BCHA and PRTN, respectively, with negligible contribution from the chelating species.

Putting the Picture Together: SERS of Genistein. Finally, the SER spectra of GSTN at various pH are shown in Figure 7. As in the derivatives BCHA and PRTN, the solid phase NR and the SER spectra have significantly different appearances. Of the three hydroxyl groups (pK_{a1} 7.2 (7-OH), pK_{a2} 10.0 (4′-OH), pK_{a3} 13.1 (5-OH)),[56] the 7-OH and 4′-OH groups are able to interact with the surface as demonstrated with BCHA and PRTN

Table 4. SERS Band Assignments for GSTN Using the Results of DFT Calculations on the 7-OH or 4′-OH Deprotonated GSTN−Ag^+ Complexes, Mode Descriptions and Their Corresponding Positions in the Neutral, Isolated GSTN Molecule[a]

experimental (cm^{-1})[b]					DFT prediction (cm^{-1})[c]					derivatives[e]	
SERS		NR[f]		Δ	[$GSTN_7$−Ag^+]	[$GSTN_{4'}$−Ag^+]	GSTN	Δ	description of [$GSTNO_7^-$−Ag^+] or [$GSTNO_{4'}^-$−Ag^+] mode[b,d]	BCHA	PRTN
265					266		274	−8	$\tau(C_9C_{10}C_4{=}O) + \tau(OC_7C_8C_9) + \tau(C_4C_{10}C_5O)$ [i]		
311	w				392		342		$\nu(Ag{-}O_7) + \tau(OC_{4'}C_{5'}C_{6'}) + \tau(C_3C_{1'}C_{6'}C_{5'})$ [i,j]	306	
311	w					296		−46	$\nu(Ag{-}O_{4'}) + \tau(OC_{4'}C_{5'}C_{6'})$ [i]		319
419	m	409	m	10	391		392	−1	$\tau(C_9O_1C_2C_3) + \tau(OC_{4'}C_{5'}C_{6'}) + \tau(C_3C_{1'}C_{2'}C_{3'})$ [i]	429	
499	m	493	w	6		486	485	1	$\tau(C_2C_3C_{1'}C_{2'}) + \tau(C_5C_{10}C_4{=}O) + \delta(C_8C_9O_1) + \delta(C_{3'}C_{4'}O)$ [i]		499
519	w					518			$\gamma(CCC)^{16b}_{B\alpha} + \delta(C_9O_1C_2) + \delta(C_3C_4C_{10}) + \nu(Ag{-}O_{4'})$ [k,o]		512
537	w	533		4		535	526	9	$\gamma(CCC)^{16b}_{B\alpha} + \nu(Ag{-}O_{4'})$ [k,o]		542
570	w	566	m	10	569		559	10	$\gamma(CCC)^{16b}_{B\alpha} + \delta(C_6C_7O) + \delta(C_4{=}O) + \delta(OC_5C_6) + \nu(Ag{-}O_7)$ [o]	568	
570	w	566	m	10		569		10	$\delta(OC_5C_6) + \delta(C_2C_3C_4) + \gamma(CCC)^{16b}_{B\alpha} + \nu(Ag{-}O_{4'})$ [k,o]		568
606	m	619	w	−13	604		614	−10	$\delta(C_6C_7C_8) + \delta(C_{2'}C_{3'}C_{4'}) + \delta(C_{4'}OC_{Me}) + \nu(Ag{-}O_7)$	602	
630	s				626		610	16	$\delta(C_6C_7C_8) + \delta(C_{4'}C_{5'}C_{6'}) + \nu(C_{1'}{-}C_3) + \nu(Ag{-}O_7)$	625	
630	s	–	–			615		5	$\tau(HC_6C_5C_{10}) + \tau(C_2O_1C_9C_{10}) + \delta(OC_7C_8) + \delta(C_4{=}O) + \nu(Ag{-}O_4{'})$ [k,l]		629
643	s				645		630	15	$\tau(C_6C_7C_8H) + \tau(OC_5C_6H)$ [i]	641	
656	s	650	w	6		652	644	8	$\delta(C_{4'}C_{5'}C_{6'}) + \delta(C_{1'}C_{2'}C_{3'}) - (O_1C_9C_{10}) + \nu(Ag{-}O_{4'})$ [k]		661
700	vw	701	vw	−1		688	682	6	$\gamma(CCC)^4_A + \tau(C_{1'}C_3C_4{=}O)$		703
727	vw	725	w	2	713		712	1	$\gamma(CCC)^4_B$	726	
727	vw	725	w	2		716		4			728
791	vs	789	vs	2		776	778	−2	$\gamma(C_6{-}H) + \tau(C_{2'}C_3C_4{=}O) + \delta(C_2O_1C_9)$		782
791	vs	789	vs	2	780			2		778	
824	m	820	m	4		833	819	14	$\delta(C_{2'}C_{1'}C_{6'}) + \nu(C_{4'}{-}O) + \nu_{sym}(C_{3'}{-}C_{4'}, C_{4'}{-}C_5{'})$		824
872	vw	883	s	−11		872	874	−2	$\delta(O_1C_2C_3) + \delta(C_4{=}O) + \nu(C_5{-}C_{10}) + \gamma(5\text{-}OH) + \delta(CCC)^1_B$		876
883	vw			0	877			3	$\delta(O_1C_2C_3) + \delta(C_4{=}O) + \nu(C_5{-}C_{10}) + \delta(CCC)^1_B$	882	
981	w	991	s	−10	977	984	985	−8	$\nu_{sym}(C_6{-}C_7, C_7{-}C_8) + \nu_{sym}(C_9{-}O_1, O_1{-}C_2) + \nu(C_7{-}O)$	981	
1006	vw					998	1009	−11	$\delta(C{-}H)^{18a}_{B\alpha}$		1005
1041	vw	1046	w	−5		1043	1044	−1	$\nu(O_1{-}C_2) + \nu(C_3{-}C_4)$ [m]		1020
1058	w	1062	m	−4	1053		1056	−3	$\nu(O_1{-}C_9) - \nu(C_3{-}C_4) + \delta(C_2{-}H)$	1060	
1140[g]	m	1145	vw	−8	1160		1148	12	$\delta(C_8{-}H) + \nu(C_7{-}O)$	1142	
1169	s	1179	w	−10		1177	1185	−8	$\delta(C{-}H)^{9a}_{B\alpha} + \delta(7\text{-}OH) + \delta(C_6{-}H)$		1172
1187	w			8	1184			−1	$\delta(C{-}H)^{9a}_{B\alpha}$	1182	
1204	sh,w				1214		1232	−18	$\delta(C_8{-}H) + \nu_{asym}(O_1{-}C_2, C_4{-}C_{10})$	1205	
1228	vs					1288	1267	21	$\nu(C_{4'}{-}O)$ [n]		1232
1255	m	1251	m	4	1257		1260	−3	$\nu(C_3{-}C_{1'}) - \nu_{sym}(O_1{-}C_2, C_4{-}C_{10}) - \nu(C_7{-}O)$	1257	
1255	m	1251	m	4		1260		0	$\nu(C_3{-}C_{1'}) - \nu(O_1{-}C_2) + \delta(7\text{-}OH)$		1255
1289	m,sh					1274	1302	−28	$\nu_{asym}(C_{1'}{-}C_{6'}, C_{1'}{-}C_{2'}) + \nu_{asym}(C_{3'}{-}C_{4'}, C_{4'}{-}C_{5'}) + \nu(C_4{'}\text{-}O)$		1291
1301	s	1306	m	−5	1306		1314	−8	$\delta(C_2{-}H) + \nu(C_{1'}{-}C_3) + \nu(C{=}C)^{14}_A + \delta(C_{2'}{-}H)$	1293	
1311	s	1317	m	−6	1324		1326	−2	$\nu_{asym}(C_4{-}C_{10}, C_5{-}C_{10}) + \delta(C_8{-}H) + \delta(C_2{-}H) + \nu(C_5{-}O) + \nu(C_7{-}O)$	1314	

dx.doi.org/10.1021/jp207730g | J. Phys. Chem. B 2011, 115, 13943–13954

Table 4. Continued

experimental (cm^{-1}) [b]				DFT prediction (cm^{-1}) [c]				derivatives [e]	
SERS	NR [f]	Δ	$[GSTN_7{-}Ag^+]$	$[GSTN_{4'}{-}Ag^+]$	GSTN	Δ	description of $[GSTNO_7^-{-}Ag^+]$ or $[GSTNO_{4'}^-{-}Ag^+]$ mode [b,d]	BCHA	PRTN
1355 w	1400* w	−45	1375		1400	−25	$\nu_{asym}(C_6{-}C_7, C_7{-}O) + \nu(C_3{-}C_4) + \delta(C_2{-}H)$	1357	
1404 w			1418		1422	−4	$\nu_{sym}(C_7{-}O, C_5{-}O) + \nu_{asym}(C_3{-}C_4, C_4{-}C_{10}) + \delta(5O{-}H)$	1407	
1477 m	1504*	−27	1479		1510	−31	$\nu(C{=}C)^{19a}_{A\alpha} + \delta(5O{-}H) + \nu(C_7{-}O)$ [n,o,p]	1476	
1492 s	1517 vw	−25		1496	1525	−29	$\nu(C{=}C)^{19a}_{B\alpha} + \nu(C_{4'}{-}O)$ [n,o,p]		1495
1556 w	1581	−25	1549		1586	−37	$\nu(C{=}C)^{8b}_{A\beta} + \delta(5O{-}H)$	1554	
1593 s	1623 vs	−30		1606	1630	−26	$\nu(C{=}C)^{8a}_{B\alpha} + \nu(C_4{=}O) - \nu(C_2{=}C_3)$ [n,o]		1594
1606 [h]		−17	1629			−1	$\nu(C{=}C)^{8a}_{B\alpha}$ [o]	1612	
1648 m	1649 s	−1	1658		1661	−3	$\nu(C{=}C)^{8a}_{A\alpha} + \nu(C_2{=}C_3) + \delta(5\text{-}OH)$ [o]	1651	
1648 m	1649 s	−1		1661		0			1653

[a] The corresponding BCHA or PRTN bands are also shown. [b] Labels and notations as per Table 1. [c] All DFT predicted wavenumbers have been scaled uniformly by a factor of 0.9790. [d] Some modes are slightly different to the equivalent NR description. In such cases, preference is given to a more accurate description of the analyte complex. [e] The equivalent experimental SERS band of BCHA or PRTN. As per NR modes, some may be different and preference is given to the appropriate GSTN complex. [f] The NR peaks are those observed from a dried solid sample, except those marked with *, which is from the IR spectrum. [44] [g] The shifts here appear to be in the opposite directions but can unambiguously be assigned to this mode relative to the surrounding peaks. The same behavior is observed in BCHA. [h] Hidden peak revealed by a curve fit and the second derivative spectrum. [i] See Table 1. [j] Output lists the internal hydrogen bonding "stretch" between 5-OH hydrogen and the carbonyl oxygen to be the largest contribution. [k] NR equivalent modes are slightly different due to $\nu(Ag{-}O_{4'})$ contribution. [l] This mode is slightly coupled to an adjacent mode predicted at 617 cm^{-1}. [m] Appears like $\delta(CCC)_C$. [n] Using Suter's description [57] for phenolate anion: ν_4 = 1593 cm^{-1}, ν_5 = 1492 and 1477 cm^{-1}, and ν_6 = 1228 cm^{-1}. [o] The motions appear as (CCC + CH). [p] Vibration degenerate according to Scherer.

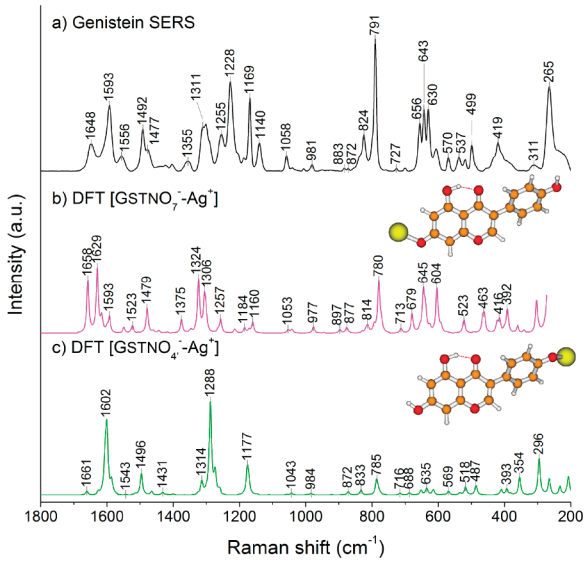

Figure 9. Experimental SERS of GSTN (a) and the DFT simulated Raman spectra of the deprotonated GSTN−Ag^+ complex interacting via (b) $C_7{-}O^-$ and (c) $C_{4'}{-}O^-$ oxygens, labeled $[GSTNO_7^-{-}Ag^+]$ and $[GSTNO_{4'}^-{-}Ag^+]$, respectively.

respectively, whereas 5-OH appears to be inactive on the surface as a binding site. Accordingly, the SER spectrum of GSTN appears almost as a sum of the spectra of the two derivatives, facilitating a comparative assignment of the observed bands (Figure 8 and Table 4). Characteristic peaks at 1492 and 1477 cm^{-1} of the phenolic ν_5-type modes at ring B ($C_{4'}$-O^-) and ring A ($C_7{-}O^-$) clearly show the anionic nature of GSTN as it interacts with the metal surface. The prominent peaks of BCHA at 1651, 1476, 1307 (overlapped bands), 1142, 1060, and 641 cm^{-1} correlate convincingly with 1648, 1477, 1311 (overlapped bands), 1140, 1058, and 643 cm^{-1} peaks of GSTN, respectively. These peaks were assigned using the GSTN anion−Ag^+ complex $[GSTNO_7^-{-}Ag^+]$ as shown in Figure 9, directly analogous to the BCHA anion−Ag+ complex, $[BCHAO_7^-{-}Ag^+]$. Similarly, peaks assignable to the alternative $[GSTNO_{4'}^-{-}Ag^+]$ complex are present at 1593, 1492, 1228 (poorly predicted), 1169, and 824 cm^{-1}, all of which feature dominantly in SERS of PRTN at 1594, 1495, 1232, 1172, and 824 cm^{-1}, respectively. This behavior is also in agreement with the daidzein spectrum, which shows multiple interactions with the surface.[10] The final rms error based on the assignments through the two proposed complexes was 13.5 cm^{-1}, or 10.6 cm^{-1} without the sensitive C−O stretch as in PRTN. It should be noted that the simultaneous attachment of $Ag^{0/+}$ at the two positions did not improve the agreement between the DFT prediction and the experimental SERS, and it is thus proposed that the two interactions occur independently

CONCLUSION

Surface-enhanced Raman spectroscopy characterization of isoflavones have been extended to include 5-hydroxy substituted analogues; genistein, biochanin A, prunetin, and 4′,7-dimethoxygenistein. The SER spectral assignments have been achieved by means of a comparative analysis of the four isoflavones, as well as phenol and other flavonoid compounds. DFT calculations on the analyte−metal complex have again been demonstrated to be a

useful approach to understanding the interfacial interactions in SERS analysis through predicted wavenumber shifts. Through this work, we have identified the interaction of the hydroxyisoflavones as anions, deprotonated at the C_7- and $C_{4'}$—OH groups, whereas the C_5—OH group is found to have little contribution to the analyte—metal interaction in SERS. Although more research may be required before a reliable application of SERS for isoflavones can be realized, this work sheds light on the interaction of isoflavones with Ag nanoparticles and shows an effective approach to SERS analysis of this particular group of molecules.

■ ASSOCIATED CONTENT

Supporting Information. Structures of the chelated species of genistein and derivatives, together with the DFT simulations of Raman spectra are shown in Figures S1—S4. This material is available free of charge via the Internet at http://pubs.acs.org.

■ AUTHOR INFORMATION

Corresponding Author

*Telephone: +61-3-9905-4552. Fax: +61-3-9905-4597. E-mail: Donald.McNaughton@monash.edu.

■ ACKNOWLEDGMENT

We thank the National Computational Infrastructure (NCI) National Facility and the Monash Sun Grid (MSG) at the Monash e-Research Centre for computational facilities, the Australian Government, and the Monash Research Graduate School (MRGS) for postgraduate scholarship support. We also acknowledge the invaluable assistance of Mr. Finlay Shanks with spectroscopic instrumentation.

■ REFERENCES

(1) Fleischmann, M.; Hendra, P. J.; McQuillan, A. J. *Chem. Phys. Lett.* **1974**, *26*, 163–166.
(2) Albrecht, M. G.; Creighton, J. A. *J. Am. Chem. Soc.* **1977**, *99*, 5215–5217.
(3) Jeanmaire, D. L.; Van Duyne, R. P. *J. Electroanal. Chem.* **1977**, *84*, 1–20.
(4) Lombardi, J. R.; Birke, R. L. *J. Phys. Chem. C* **2008**, *112*, 5605–5617.
(5) Aroca, R. *Surface-Enhanced Vibrational Spectroscopy*; John Wiley & Sons, Ltd.: West Sussex, U.K., 2006.
(6) Smith, E.; Dent, G. *Modern Raman Spectroscopy*; John Wiley & Sons Ltd.: West Sussex, U.K., 2005.
(7) Kennedy, B. J.; Spaeth, S.; Dickey, M.; Carron, K. T. *J. Phys. Chem. B* **1999**, *103*, 3640–3646.
(8) Lombardi, J. R.; Birke, R. L.; Lu, T.; Xu, J. *J. Phys. Chem.* **1986**, *84*, 4174–4180.
(9) Morton, S. M.; Jensen, L. *J. Am. Chem. Soc.* **2009**, *131*, 4090–4098.
(10) Sekine, R.; Vongsvivut, J.; Robertson, E. G.; Spiccia, L.; McNaughton, D. *J. Phys. Chem. B* **2010**, *114*, 7104–7111.
(11) Gültekin, E.; Yildiz, F. Introduction to Phytoestrogens. In *Phytoestrogens in Functional Foods*; Yildiz, F., Ed.; CRC Press: Boca Raton, FL, 2006; pp 3—18.
(12) Karahalil, B. Benefits and Risks of Phytoestrogens. In *Phytoestrogens in Functional Foods*; Yildiz, F., Ed.; CRC Press: Boca Raton, FL, 2006.
(13) Jackman, K. A.; Woodman, O. L.; Sobey, C. G. *Curr. Med. Chem.* **2007**, *14*, 2824–2830.
(14) Morrissey, C.; Watson, R.; G., W. *Curr. Drug Targets* **2003**, *4*, 231–241.
(15) Usui, T. *Endocr. J.* **2006**, *53*, 7–20.
(16) Divi, R. L.; Chang, H. C.; Doerge, D. R. *Biochem. Pharmacol.* **1997**, *54*, 1087–1096.
(17) Chavarro, J. E.; Toth, T. L.; Sadio, S. M.; Hauser, R. *Hum. Reprod.* **2008**, *23*, 2584–2590.
(18) Faqi, A. S.; Johnson, W. D.; Morrissey, R. L.; McCormick, D. L. *Reprod. Toxicol.* **2004**, *18*, 605–611.
(19) Teslova, T.; Corredor, C.; Livingstone, R.; Spataru, T.; Birke, R. L.; Lombardi, J. R.; Cañamares, M. V.; Leona, M. *J. Raman Spectrosc.* **2007**, *38*, 802–818.
(20) Jurasekova, Z.; Garcia-Ramos, J. V.; Domingo, C.; Sanchez-Cortes, S. *J. Raman Spectrosc.* **2006**, *37*, 1239–1241.
(21) Corredor, C.; Teslova, T.; Canamares, M. V.; Chen, Z.; Zhang, J.; Lombardi, J. R.; Leona, M. *Vib. Spectrosc* **2009**, *49*, 190–195.
(22) Bhandari, D.; Walworth, M. J.; Sepaniak, M. J. *Appl. Spectrosc.* **2009**, *63*, 571–578.
(23) Crupi, V.; Ficarra, R.; Guardo, M.; Majolino, D.; Stancanelli, R.; Venuti, V. *J. Pharm. Biomed. Anal.* **2007**, *44*, 110–117.
(24) Mandeville, J.-S.; Froehlich, E.; Tajmir-Riahi, H. A. *J. Pharm. Biomed. Anal.* **2009**, *49*, 468–474.
(25) Crupi, V.; Majolino, D.; Paciaroni, A.; Rossi, B.; Stancanelli, R.; Venuti, V.; Viliani, G. *J. Raman Spectrosc.* **2010**, *41*, 764–770.
(26) Giese, B.; McNaughton, D. *J. Phys. Chem. B* **2002**, *106*, 101–112.
(27) Vongsvivut, J.; Robertson, E. G.; McNaughton, D. *Aust. J. Chem.* **2008**, *61*, 921–929.
(28) Vongsvivut, J.; Robertson, E. G.; McNaughton, D. *J. Raman Spectrosc.* **2010**, *41*, 1137–1148.
(29) Schreiber, M.; González, L. *J. Comput. Chem.* **2007**, *28*, 2299–2308.
(30) Dunbar, R. C. *J. Phys. Chem. A* **2002**, *106*, 7328–7337.
(31) Muniz-Miranda, M.; Gellini, C.; Pagliai, M.; Innocenti, M.; Salvi, P. R.; Schettino, V. *J. Phys. Chem. C* **2010**, *114*, 13730–13735.
(32) Papadopoulou, E.; Bell, S. E. J. *Analyst* **2010**, *135*, 3034–3037.
(33) Vivoni, A.; Birke, R. L.; Foucault, R.; Lombardi, J. R. *J. Phys. Chem. B* **2003**, *107*, 5547–5557.
(34) Cardini, G.; Muniz-Miranda, M.; Schettino, V. *J. Phys. Chem. B* **2004**, *108*, 17007–17011.
(35) Wu, D. Y.; Duan, S.; Ren, B.; Tian, Z. Q. *J. Raman Spectrosc.* **2005**, *36*, 533–540.
(36) Wu, D. Y.; Ren, B.; Jiang, Y.-X.; Xu, X.; Tian, Z. Q. *J. Phys. Chem. A* **2002**, *106*, 9042–9052.
(37) Cardini, G.; Muniz-Miranda, M.; Pagliai, M.; Schettino, V. *Theor. Chem. Acc.* **2007**, *117*, 451–458.
(38) Muniz-Miranda, M.; Pagliai, M.; Cardini, G.; Schettino, V. *J. Phys. Chem. C* **2008**, *112*, 762–767.
(39) Wu, D.-Y.; Liu, X.-M.; Duan, S.; Xu, X.; Ren, B.; Lin, S.-H.; Tian, Z.-Q. *J. Phys. Chem. C* **2008**, *112*, 4195–4204.
(40) Birke, R. L.; Znamenskiy, V.; Lombardi, J. R. *J. Chem. Phys.* **2010**, *132*, 214707.
(41) Jensen, L.; Aikens, C. M.; Schatz, G. C. *Chem. Soc. Rev.* **2008**, *2008*, 1061–1073.
(42) Zhao, L.; Jensen, L.; Schatz, G. C. *J. Am. Chem. Soc.* **2006**, *128*, 2911–2919.
(43) Lombardi, J. R.; Birke, R. L. *J. Chem. Phys.* **2007**, *126*, 244709.
(44) Sekine, R.; Robertson, E. G.; McNaughton, D. *Vib. Spectrosc.* **2011**, *57*, 306—314.
(45) Leona, M. *Proc. SPIE* **2005**, *5993*, 59930L-59931–59930L-59938.
(46) Lee, P. C.; Meisel, D. *J. Phys. Chem.* **1982**, *86*, 3391–3395.
(47) Frisch, M. J.; Trucks, G. W.; Schlegel, H. B.; Scuseria, G. E.; Robb, M. A.; Cheeseman, J. R.; J. A. Montgomery, J.; Vreven, T.; Kudin, K. N.; Burant, J. C.; Millam, J. M.; Iyengar, S. S.; Tomasi, J.; Barone, V.; Mennucci, B.; Cossi, M.; Scalmani, G.; Rega, N.; Petersson, G. A.; Nakatsuji, H.; Hada, M.; Ehara, M.; Toyota, K.; Fukuda, R.; Hasegawa, J.; Ishida, M.; Nakajima, T.; Honda, Y.; Kitao, O.; Nakai, H.; Klene, M.;

Li, X.; Knox, J. E.; Hratchian, H. P.; Cross, J. B.; Bakken, V.; Adamo, C.; Jaramillo, J.; Gomperts, R.; Stratmann, R. E.; Yazyev, O.; Austin, A. J.; Cammi, R.; Pomelli, C.; Ochterski, J. W.; Ayala, P. Y.; Morokuma, K.; Voth, G. A.; Salvador, P.; Dannenberg, J. J.; Zakrzewski, V. G.; Dapprich, S.; Daniels, A. D.; Strain, M. C.; Farkas, O.; Malick, D. K.; Rabuck, A. D.; Raghavachari, K.; Foresman, J. B.; Ortiz, J. V.; Cui, Q.; Baboul, A. G.; Clifford, S.; Cioslowski, J.; Stefanov, B. B.; Liu, G.; Liashenko, A.; Piskorz, P.; Komaromi, I.; Martin, R. L.; Fox, D. J.; Keith, T.; Al-Laham, M. A.; Peng, C. Y.; Nanayakkara, A.; Challacombe, M.; Gill, P. M. W.; Johnson, B.; Chen, W.; Wong, M. W.; Gonzalez, C.; Pople, J. A. *Gaussian 03*, revision E.01; Gaussian, Inc.: Wallingford, CT, 2004.

(48) Andrae, D.; Häußermann, U.; Dolg, M.; Stoll, H.; Preuß, H. *Theor. Chim. Acta* **1990**, *77*, 123–141.

(49) Breton, P. M.; Precigoux, G.; Courseille, C.; Hospital, M. *Acta Crystallogr., Sect. B: Struct. Sci.* **1975**, *31*, 921–923.

(50) Zhang, Z. T.; Wang, X. B.; Liu, Q. G.; Zheng, J. B.; Yu, K. B. *Acta Crystallogr., Sect. C: Cryst. Struct. Commun.* **2005**, *61*, o29–o31.

(51) Krishnakumar, V.; Keresztury, G.; Sundius, T.; Ramasamy, R. *J. Mol. Struct.* **2004**, *702*, 9–21.

(52) Scott, A. P.; Radom, L. *J. Phys. Chem.* **1996**, *100*, 16502–16513.

(53) Bell, S. E. J.; Sirimuthu, N. M. S. *J. Phys. Chem. B* **2005**, *109*, 7405–7410.

(54) Munro, C. H.; Smith, W. E.; Garner, M.; Clarkson, J.; White, P. C. *Langmuir* **1995**, *11*, 3712–3720.

(55) Guerrini, L.; Jurasekova, Z.; Domingo, C.; Pérez-Méndez, M.; Leyton, P.; Campos-Valette, M.; Garcia-Ramos, J. V.; Sanchez-Cortes, S. *Plasmonics* **2007**, *2*, 147–156.

(56) Zielonka, J.; Gebicki, J.; Grynkiewicz, G. *Free Radical Biol. Med.* **2003**, *35*, 958–965.

(57) Suter, H. U. *J. Phys. Chem. A* **1998**, *102*, 10123–10133.

(58) Nonella, M.; Suter, H. U. *J. Phys. Chem. A* **1999**, *103*, 7867–7871.

(59) Berthomieu, C.; Boussac, A. *Biospectroscopy* **1995**, *1*, 187–206.

(60) Nonella, M.; Suter, H. U. *J. Phys. Chem. A* **19981999**, *102103*, 10123−101337867–101337871.

(61) Keresztury, G.; Billes, F.; Kubinyi, M.; Sundius, T. *J. Phys. Chem. A* **1998**, *102*, 1371–1380.

(62) Sanchez-Cortes, S.; Garcia-Ramos, J. V. *J. Colloid Interface Sci.* **2000**, *231*, 98–106.

(63) Lemańska, K.; Szymusiak, H.; Tyrakowska, B.; Zieliński, R.; Soffers, A. E. M. F.; Rietjens, I. M. C. M. *Free Radical Biol. Med.* **2001**, *31*, 869–881.

(64) Dawson, R. M. C.; Elliott, D. C.; Elliott, W. H.; Jones, K. M. *Data for biochemical research*; Clarendon Press: Oxford, U.K., 1959.

(65) Cãnamares, M. V.; Garcia-Ramos, J. V.; Domingo, C.; Sanchez-Cortes, S. *J. Raman Spectrosc.* **2004**, *35*, 921–927.

(66) Cãnamares, M. V.; Sevilla, P.; Sanchez-Cortes, S.; Garcia-Ramos, J. V. *Biopolymers* **2006**, *82*, 405–409.

(67) Alcolea Palafox, M. *Int. J. Quantum Chem.* **2000**, *77*, 661–684.